

# Stagnancy of the pygmy dipole resonance<sup>\*</sup>

Xu-Wei Sun(孙旭伟)<sup>1)</sup> Jing Chen(陈靖) Ding-Hui Lu(鲁定辉)

Department of Physics, Zhejiang University, Hangzhou 310027, China

**Abstract:** The pygmy dipole resonance (PDR) of nickel isotopes is studied using the deformed random phase approximation method. The isoscalar character of the pygmy resonance is confirmed, and the correlation between the pygmy resonance and neutron skin thickness is discussed. Our investigation shows a linear correlation between PDR integral cross section and neutron skin thickness when the excess neutrons lie in pf orbits, with a correlation rate of about  $0.27 \text{ fm}^{-1}$ . However, in more neutron-rich nickel isotopes, the growth of the pygmy dipole resonance is stagnant. Although the neutron skin thickness increases, the whole skin is not active. There is an inertial part in the nuclei  $^{70-78}\text{Ni}$  which does not participate in the pygmy resonance actively and as a result, contributes little to the photo-absorption cross section.

**Keywords:** pygmy dipole resonance, axial random phase approximation, neutron skin

**PACS:** 21.60.Jz, 24.30.Gd, 27.50.+e **DOI:** 10.1088/1674-1137/42/1/014101

## 1 Introduction

The emergence of the pygmy dipole resonance (PDR) has been studied for decades, and experimental evidence has been found in many neutron-rich nuclei [1–3]. Theoretically, this low lying dipole excitation is often explained as excess neutrons at the surface region oscillating against the isospin saturated core [4, 5]. Unlike the giant dipole resonance (GDR), which is caused by highly collective coherent superposition of particle-hole excitations, the PDR appears in a much more complicated manner. The lifetime of the soft dipole mode found in  $^{11}\text{Li}$  is much shorter than that expected for a resonance peak, and this low-lying structure has been shown to be the single particle excitation of loosely bound neutrons outside the  $^9\text{Li}$  core [6]. With the increase of valence neutrons, the PDR becomes more and more collective, but it still differs from the GDR in many aspects and should not be considered as the low-energy tail of the GDR. In fact, it has been found that in the pygmy energy region, the excited states split into two different groups [7–9]. One of them has isoscalar character and can be obtained both through  $(\gamma, \gamma')$  and  $(\alpha, \alpha' \gamma)$  experiments, while the other is of isovector nature and cannot be observed in  $\alpha$  scattering. Whether this implies that the PDR has a fine structure or that the isovector part should just be considered as the low-energy tail of the GDR [10] is still an open question. In recent years, some experiments and analyses have used  $\beta$  decay as a probe to study the low-lying E1 excitation [11–13]. Such attempts can provide

additional information for this question.

The PDR has been related to much neutron-rich physics, symmetry energy and nucleosynthesis. The occurrence of the PDR is thought to enhance neutron capture rates in the r-process of nucleosynthesis and plays an important role in astrophysics [14]. The experimental results relating to the PDR can be used to constrain the slope parameter of symmetry energy [15] and further on, rule out interactions that predict too-stiff equations of state [16]. As the neutron skin thickness is sensitive to the density dependence of symmetry energy [17], it is interesting to study the correlation between the PDR and the thickness of the neutron skin. Several studies have confirmed that the fraction of EWSR (energy-weighted sum rule) exhausted by the PDR increases with the growth of neutron skin thickness [18, 19], but the correlation is not always positive. In ultra neutron excess cases, a bending structure has been suggested in many articles [16, 20].

This paper is organized as follows. We start by introducing the method we used in our investigation, namely, the axial random phase approximation, and, briefly, the formalism relating to electrical dipole excitation. Then the validation of our numerical approach and convergence checks are presented. We discuss the emergence of the pygmy dipole resonance in nickel isotopes and compare PDR and GDR in different aspects, e.g., their isospin character and collectivity. The correlation between the fraction of PDR integral cross section and neutron skin thickness is studied. The phenomenon of

Received 23 June 2017, Published online 15 November 2017

<sup>\*</sup> Supported by National Science Foundation of China

1) E-mail: snowsxw@zju.edu.cn

©2018 Chinese Physical Society and the Institute of High Energy Physics of the Chinese Academy of Sciences and the Institute of Modern Physics of the Chinese Academy of Sciences and IOP Publishing Ltd

PDR stagnancy is discussed and its physical mechanism is shown in the last part.

## 2 Method

In the relativistic meson-exchange model, the mean field is provided by the cancellation between the scalar potential provided by the  $\sigma$  meson and the vector potential provided mainly by the  $\omega$  meson. Isospin and electrical information are interpreted by the iso-vector meson  $\vec{\rho}$  and the photon. In the mean field approximation, the two-body interaction reads

$$V(\mathbf{r}_1, \mathbf{r}_2) = -g_\sigma \beta^1 G_\sigma(\mathbf{r}_1, \mathbf{r}_2) g_\sigma \beta^2 + g_\omega G_\omega(\mathbf{r}_1 - \mathbf{r}_2) g_\omega + g_\rho \tau_3^1 G_\rho(\mathbf{r}_1 - \mathbf{r}_2) g_\rho \tau_3^2 + e^2 \frac{1 - \tau_3^1}{2} G_\gamma(\mathbf{r}_1 - \mathbf{r}_2) \frac{1 - \tau_3^2}{2}, \quad (1)$$

where  $g_{\sigma, \omega, \rho}$  is the coupling constant of the related interaction vertex, and can be obtained by fitting the bulk properties of infinite nuclear matter and finite nuclei. The meson propagators have the Yukawa form except for  $\sigma$ , because it is crucial to introduce its self-coupling in order to get reasonable nuclear incompressibility [21]. The propagator of  $\sigma$  meson can be calculated from the Klein-Gordon equation (assuming the self interaction of the  $\sigma$  meson is  $U(\sigma)$ ):

$$(-\Delta + m_\sigma^2 + U''(\sigma)) G_\sigma(\mathbf{r}_1, \mathbf{r}_2) = -\delta(\mathbf{r}_1 - \mathbf{r}_2). \quad (2)$$

The energy density functional of the nucleus is

$$E[\rho] = \text{Tr}(\epsilon \rho) + \frac{1}{2} \text{Tr} \text{Tr}(\rho V \rho), \quad (3)$$

where  $\epsilon$  is the kinetic energy. In the small amplitude limit, the density operator reads

$$\rho(t) = \rho^0 + \delta\rho(\omega) e^{-i\omega t} + \delta\rho^\dagger(\omega) e^{i\omega t} \quad (4)$$

and its time evolution obeys [22]

$$i\partial_t \hat{\rho} = [\hat{h}^0, \delta\hat{\rho}] + [\delta\hat{h}, \hat{\rho}^0]. \quad (5)$$

The static Hamiltonian and density have extremely simple forms in single particle space, i.e.,  $h_{kl}^0 = \epsilon_k \delta_{kl}$ ,  $\rho_{kl}^0 = \rho_k \delta_{kl}$ , where  $\rho_k = 1$  for 'hole' states, and  $\rho_k = 0$  for 'particle' states. As a projector operator,  $\hat{\rho}^2 = \hat{\rho}$  holds all the time, which means the non-vanishing transition densities are  $\delta\rho_{ph}$  and  $\delta\rho_{hp}$ . Substituting the explicit expression of

$$\delta h = \frac{\partial h}{\partial \rho} \delta \rho = \sum_{ph} \frac{\partial h}{\partial \rho_{ph}} \delta \rho_{ph} + \sum_{hp} \frac{\partial h}{\partial \rho_{hp}} \delta \rho_{hp}, \quad (6)$$

into Eq. (5), we can get coupling equations for  $\delta\rho_{ph}$  and  $\delta\rho_{hp}$ , which can be expressed in a much more compact form

$$\begin{pmatrix} A & B \\ B^* & A^* \end{pmatrix} \begin{pmatrix} X \\ Y \end{pmatrix} = \omega \begin{pmatrix} 1 & 0 \\ 0 & -1 \end{pmatrix} \begin{pmatrix} X \\ Y \end{pmatrix}, \quad (7)$$

if we introduce

$$\begin{aligned} A_{php'h'} &\equiv (\epsilon_p - \epsilon_h) \delta_{pp'} \delta_{hh'} + V_{ph'hp'} \\ B_{php'h'} &\equiv V_{pp'hh'} \end{aligned}, \quad (8)$$

where X, Y denote  $\delta\rho_{ph}$  and  $\delta\rho_{hp}$  respectively, and the matrix elements of residual interaction are defined by

$$V_{abcd} \equiv \frac{\partial h_{ac}}{\partial \rho_{db}}. \quad (9)$$

In the above equations, we have included the antiparticle states as 'p' for simplicity, which is essential for the consistent description of excitation states.

Pairing correlations have important effects on superfluid nuclei [23]. A consistent framework based on Hartree-Bogoliubov ground states, the quasiparticle random phase approximation (QRPA) model, has previously been developed [24]. Due to huge configurations in the deformed case, QRPA calculations are mostly implemented in spherical symmetry [25], except for the work by Arteaga et al. [26]. A severe energy cutoff for the two quasiparticle pairs (typically less than 60 MeV) has to be used to limit the configurations. The price to pay is that the spurious states cannot be decoupled completely. Since the PDR is seemingly the interplay of the neutron excess, shell effects, deformation and pairing, early relativistic RPA calculations tend to neglect the pairing [16], as does a recent systematic RPA study of the PDR in light to medium nuclei with Skyrme interaction [20]. Indeed, a canonical QRPA calculation has shown that the pairing correlations do not significantly affect the soft E1 strength distribution [25]. Therefore we choose the deformed framework and neglect the pairing interaction in this work.

After diagonalizing Eq. (7) we will get the energy and transition density of each excited state, which enables us to access the transition amplitude of a particular operator  $\hat{F}$

$$\langle 0 | \hat{F} | \nu \rangle = \sum_{ph} \hat{F}_{hp} X_{ph}^\nu + \hat{F}_{ph} Y_{ph}^\nu. \quad (10)$$

The electrical dipole operator is [22]

$$\hat{E}_{1\mu} = \frac{N}{N+Z} \sum_{p=1}^Z r_p Y_{1\mu} - \frac{Z}{N+Z} \sum_{n=1}^N r_n Y_{1\mu}, \quad (11)$$

and the excitation strength can be evaluated by the reduced transition probability

$$B(E1, \omega_\nu) = 3 |\langle \nu | \hat{E}1 | 0 \rangle|^2. \quad (12)$$

The photo absorption cross section reads [27]

$$\sigma(\omega) = \frac{16\pi^3 e^2}{9\hbar c} \omega R(\omega), \quad (13)$$

where the response function  $R(\omega)$  is often smeared by a Lorentzian function with width  $\Gamma$ .

$$R(\omega) = \sum_\nu B(E1, \omega_\nu) \frac{1}{\pi} \frac{\Gamma/2}{(\omega - \omega_\nu)^2 + (\Gamma/2)^2}. \quad (14)$$

In our calculations,  $\Gamma$  is taken to be 1 MeV.

### 3 Validation of numerical implementation

Although the random phase approximation (RPA) method has been established and developed for years [28–30], only in the last decade has application in non-spherical symmetry become practical [31]. In the axial symmetry case, the angular momentum projection  $K$  and parity  $\pi$  are conserved, and the configuration space of particle-hole pairs can be built according to the selection rule  $\Omega_p - \Omega_h = K$ ,  $\pi_p \pi_h = \pi$ , where  $\Omega_i^{\pi_i}$  is the quantum number of a single particle state.

In relativistic models, although the antiparticle states are neglected when calculating nucleus densities, i.e., no sea approximation [32], they are essential ingredients for describing the excitation properties, including the decoupling of spurious states from physical ones. The spurious states correspond to the restoration of rotational and translational symmetry broken by mean field treatment. They are Nambu-Goldstone bosons accompanied by spontaneous symmetry breaking and have vanishing energies if the numerical approach is precise. However, such an ideal situation never happens in real calculations. The spurious state always stay a little higher than 0 and can be regarded as an indicator of numerical veracity.

Besides the energies of spurious states, it is very important to know whether they are mixed with physical

states. The nature of these states make them the dominant contributors to the corresponding symmetry operators. Meanwhile, the ratio of forward amplitude and backward amplitude  $d \equiv |X|^2/|Y|^2$  is close to zero for physical states because the RPA ground state is not far from the relativistic mean field (RMF). However, for spurious states, which represent the collective motion of the nucleus as a whole,  $d \approx 1$ . Figure 1 shows the response to the Goldstone boson generator  $\hat{P}_0$ ,  $\hat{P}_+$  (linear momentum operator) and  $\hat{J}_+$  (angular momentum operator) in the nucleus  $^{76}\text{Ni}$ . The quantum number and position of spurious states  $E_s$  as well as the amplitude ratio  $d$  are labeled in each panel. The energies of the Goldstone bosons are very close to zero. In this particular calculation they are 0.076 MeV, 0.057 MeV and 0.049 MeV for translation and rotation spurious states respectively. For the rest of the Ni isotopes, the positions of spurious states are no higher than 0.2 MeV, and are all well separated from physical ones in our calculation. In the lower right corner of Fig. 1, we give a convergence check of the only truncation used in our calculation, i.e., the maximum quantum number of major shell  $N_F$ , which remains the same in RMF and RPA levels in order to keep self-consistency. It is clear that, as  $N_F$  changes from 16 to 18, the strength function varies in a negligible way, especially in the PDR region. Therefore, we choose  $N_F = 16$  in our calculation, and in such a case, the number of 1p1h pairs is roughly ten thousand.

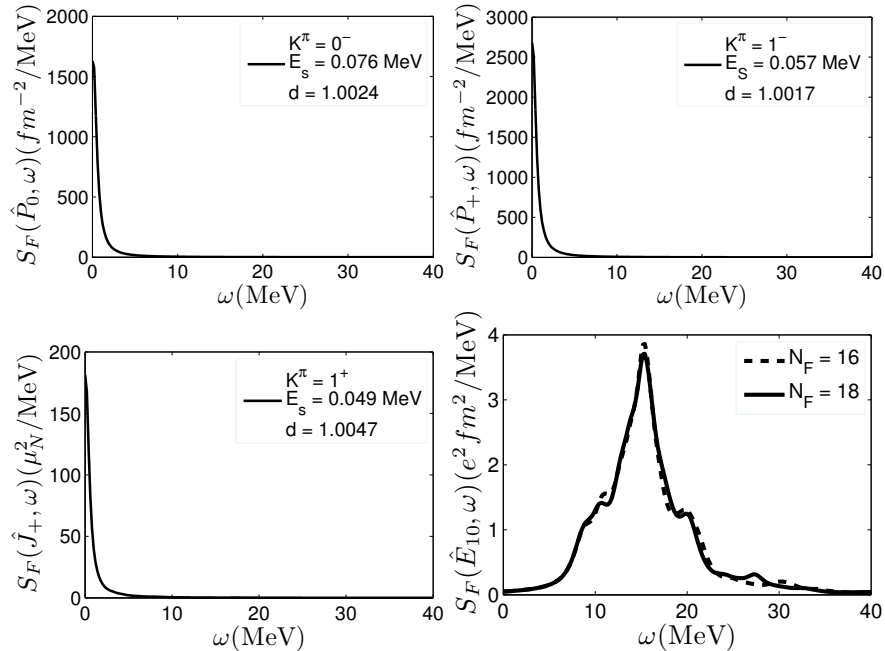


Fig. 1. The response of the nucleus  $^{76}\text{Ni}$  to translation and rotation operators as well as the convergence check of maximum oscillator quantum number  $N_F$ . The strength functions for the E1 operator in the  $K^\pi=0^-$  channel are smeared with  $\Gamma=2$  MeV.

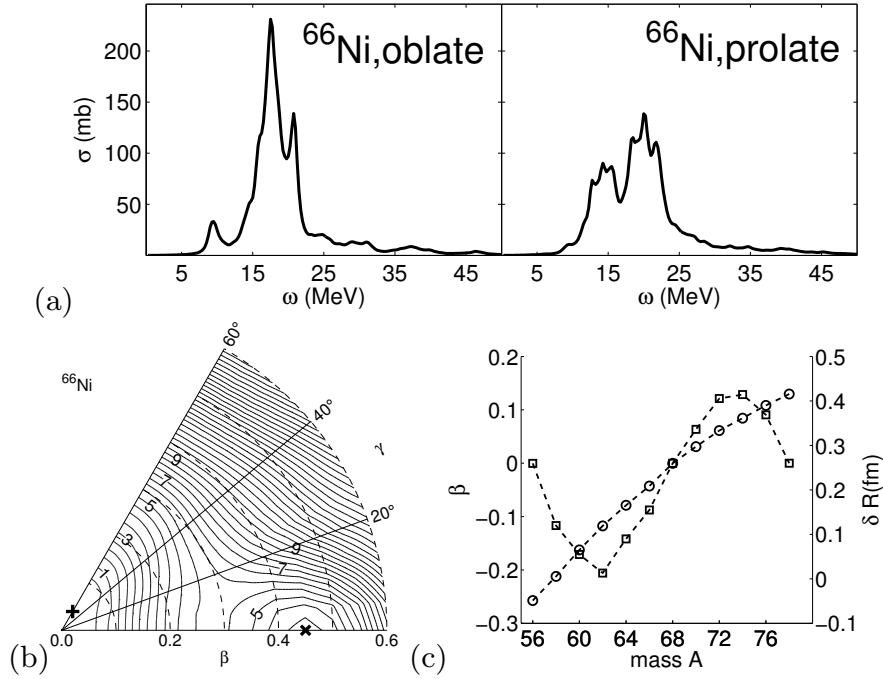


Fig. 2. (a) The deformation effect on photo-absorption cross section. (b) Potential-energy surface expressed with contours spaced by 0.5 MeV ( $\beta, \gamma$  are Hill-Wheeler coordinates). (c) Deformation and neutron skin thickness of nickel isotopes. The former (squares) is scaled on the left axis, and the latter (circles) on the right.

In our calculations, the deformations of nuclei are determined from a self-consistent procedure by using different initial basis parameters, which is equivalent to setting the initial potential to a particular shape. Such a procedure will reach a local minimum in the potential-energy surface/curve (PES), and for most nuclei, this is their ground state. For the Ni isotopes we study, besides the ground state, there exists a secondary minimum in some nuclei. If the RPA calculation are performed on such a state, the strength function will be very different from that performed on a true ground state. In Fig. 2(a) we show the results of such a case in  $^{66}\text{Ni}$ , which has a prolate shape-coexistence isomeric state with  $\beta \approx 0.45$  besides the ground state with  $\beta \approx -0.08$ . The cross sections change in a significant way in these two geometries. The PDR is severely hindered in the isomeric case. Such a comparison shows that the deformation has a prominent effect on the PDR and should not be omitted. In our calculation, the deformation of nuclei is carefully checked and guaranteed to be the ground state predicted by the model. In nickel isotopes, only  $^{56}\text{Ni}$ ,  $^{68}\text{Ni}$  and  $^{78}\text{Ni}$  are spherical. The deformation parameter  $\beta$  of the others range from -0.2 to 0.1. We have illustrated explicitly the deformation values as well as the neutron skin thickness of Ni isotopes in Fig. 2(c). The PES in Fig. 2(b) shows the ground state as well as the shape isomeric state in  $^{66}\text{Ni}$ , which is generated by using the triaxial constraint RHB solver DIRHB [33]. The deformations of ground and isomeric states (marked by '+' and 'X', respectively)

are compatible with the results of the non-linear meson model we used.

## 4 Results

### 4.1 Isospin Characteristics of PDR

In Fig. 3(a) we show our calculated photo-absorption cross section for  $^{60}\text{Ni}$ . Apart from the wide peak of the GDR, a small peak emerges at the energy region about 10 MeV, which is the PDR. Besides the amplitude and energy region, the isospin characteristics of the GDR and PDR are different. Here we use the IS percentage to indicate the isospin character of a excited state, which can be obtained by counting the percentage of in-phase oscillation region of neutrons and protons [34]. When a partial cross section contains excitations with  $0 < \text{IS} < x$ , we label it by  $\text{IS} < x$ . As  $x$  decreases,  $\text{IS} < x$  rules out isoscalar components, while  $\text{IS} > x$  has the opposite effect. The peaks of the GDR and PDR can easily be picked out through different IS curves. The wide peak of the GDR, centered at about 18 MeV, mainly consists of the superposition of excited levels with  $\text{IS} < 0.6$ , which means this resonance structure originates from the out-phase-oscillation of neutrons and protons. Meanwhile, the pygmy resonance is in-phase-oscillation dominant. It survives even under the stringent restriction  $\text{IS} > 0.75$ , which strongly indicates the isoscalar character of the pygmy resonance.

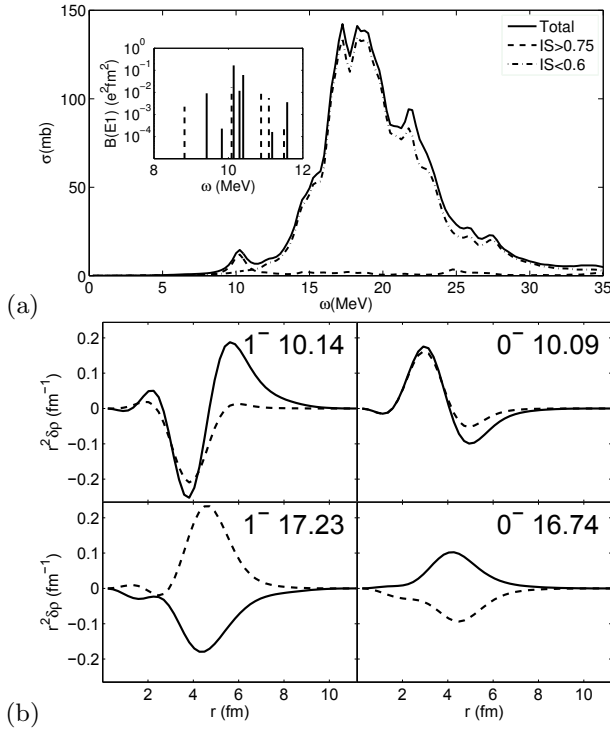


Fig. 3. (a) Photo-absorption cross section for  $^{60}\text{Ni}$ . Cross sections with different isospin character are expressed with different IS curves. The inset figure focuses on the pygmy resonance region, containing the electrical dipole transition probabilities of  $^{60}\text{Ni}$ . The solid lines represent the results in the  $K^\pi=1^-$  configuration, while dashed lines are for  $K^\pi=0^-$ . (b) Radial distribution of transition densities of dominant excited levels in the energy region of PDR and GDR in  $^{60}\text{Ni}$ . The quantum number of each level ( $K^\pi$ ) and excited energy in MeV are shown in the upper right corner of each panel. The solid (dashed) line indicates the transition density of neutrons (protons).

In the inset of Fig. 3(a), we show the E1 transition probabilities in the PDR region. In the case of axial symmetry, the response involves the  $K=\pm 1$  and  $K=0$  channels, where  $K$  is the angular momentum projection on the z-axis. For spherical nuclei, the response of the three different channels are coincident, while for deformed nuclei, the dipole strength splits into different parts. In  $^{60}\text{Ni}$ , the prominent PDR peak originates from the 10.14 MeV and 10.40 MeV states in the  $K^\pi=1^-$  channel and 10.09 MeV in the  $K^\pi=0^-$  channel. Although there are other excited levels, their transition strengths are much smaller. For a given excited state  $\nu$ , the contribution of a particular particle-hole pair can be measured through

$$C_{ph}^\nu = |X_{ph}^\nu|^2 - |Y_{ph}^\nu|^2. \quad (15)$$

The levels mentioned above can be explained as excitations of the excess neutrons in orbits  $\frac{3}{2}^-$  [301] and  $\frac{5}{2}^-$  [303] (the digits in brackets are the quantum numbers

of the major oscillator component [32]), contributing a great proportion, about 70%–80% ( $\sum_p C_{ph}^\nu$ ). The transition densities of leading states in the PDR and GDR have typical radial distribution patterns, i.e., in-phase or out-of-phase. From Fig. 3(b), in the PDR case, the neutron density and proton density mostly have the same sign all over the region, and in the surface region, there is a large tail from excess neutrons. This is the reason that the PDR is sometimes called ‘skin mode’ [35]. In the GDR case, the situation is completely opposite: protons and neutrons oscillate out-of-phase against each other.

## 4.2 Stagnancy of PDR in Ni isotopes

In the nickel isotopic chain, the significant PDR first appears in  $^{60}\text{Ni}$ . When neutron number increases, the amplitude of the PDR grows accordingly, as shown in Fig. 4(a). However, for nuclei  $^{70-76}\text{Ni}$ , the peak of the PDR cannot be separated nicely from the whole spectrum. There is a transition region where the PDR and the low energy tail of the GDR may overlap. To date, the energy region of the PDR lacks a conclusive definition. Some researchers use 10 MeV as the upper limit [4, 20, 26], but others defines the ‘pygmy transition energy’ as 11.25 MeV [27], or restrict it to below the neutron emission threshold [36]. Therefore, in our calculation, when there is a transition area, the PDR will be checked by using different intervals.

Here, we introduce a coefficient

$$R_h^k = \frac{\sum_{\nu \in E} B(E1, \omega_\nu) \varepsilon_\nu^k \sum_p C_{ph}^\nu}{\sum_{\nu \in E} B(E1, \omega_\nu) \varepsilon_\nu^k} \quad (16)$$

to indicate the contribution of a ‘hole’ state to the  $k$ th energy weighted sum rule in the energy region  $\nu \in E = [E_{\min}, E_{\max}]$ . It is easy to see the normalization condition is  $\sum_h R_h^k = 1$ . The square sum is defined as

$$S_c = \sum_h (R_h^1)^2. \quad (17)$$

In extreme conditions, for a single particle excitation,  $S_c=1$ , while for a fully collective resonance the strength is averaged over each nucleon equally,  $S_c \approx \sum (1/A)^2 = 1/A$ , where  $A$  is the mass number. In this manner, the smaller  $S_c$  is, the more collective a resonance should be. Therefore,  $S_c$  can be regarded as an indicator of a resonance’s collectivity. In Fig. 4(b), we compare the collectivity of the GDR and PDR in nickel isotopes. In the GDR region, the resonance is highly collective, with a small  $S_c$  which lies below 0.1, while in the PDR case,  $S_c$  is larger. Pygmy resonances are less collective than giant resonances. This result is consistent with Ref. [37], although different indicators are used. With the increase of excess neutrons, the  $S_c$  value belonging to PDR declines from 0.52 to about 0.2, which means the resonance becomes more and more collective. However, we also

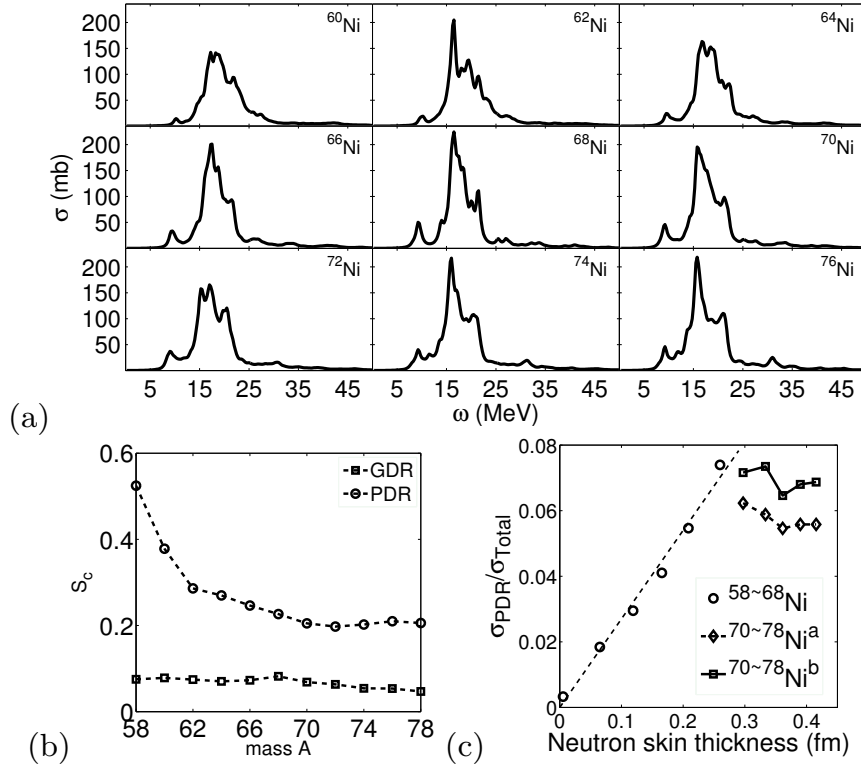


Fig. 4. (a) Photo-absorption cross section for Ni isotopes. The smearing width is taken to be 1 MeV. (b)  $S_c$  of PDR are expressed by squares and PDR by circles. (c) The relationship between neutron skin thickness and pygmy cross section fraction in nickel isotopes. The isotopes with pygmy resonance are grouped into two chains. The first is marked by circles and contains  $^{58-68}\text{Ni}$ . The second, marked by diamonds/squares, contains  $^{70-78}\text{Ni}$ .  $\text{Ni}^a$  represents the result corresponding to energy cutoff 10 MeV, and  $\text{Ni}^b$  to that for 11 MeV, see text for details. The dashed straight line represents a linear fit between neutron skin thickness and fraction of PDR related integral cross section.

notice that in nuclei  $^{70-78}\text{Ni}$ ,  $S_c$  floats in a narrow region near 0.2, and the collectivity of pygmy resonance does not increase. To some extent it shows that some excess neutrons in these nuclei do not participate actively in the pygmy dipole resonance. We call them ‘pygmy inertial excess neutrons’ (PIEN).

A strong correlation between the energy weighted sum rule being exhausted by the pygmy resonance and neutron excess has been suggested in some studies [18, 27]. In order to investigate the effect of PIEN, in Fig. 4(c), we illustrate the evolution of the PDR’s integral cross section with the growth of neutron skin thickness. When the excess neutrons increase, the evolution exhibits two distinct patterns. In the nickel isotope chain  $^{58-68}\text{Ni}$ , a linear correlation between the fraction of PDR integral cross section and the thickness of neutron skin has been confirmed in our calculation

$$\frac{\sigma_{\text{PDR}}}{\sigma_{\text{Total}}} \approx 0.27\delta r, \quad (18)$$

where  $\delta r$  is neutron skin thickness and the coefficient has dimension  $\text{fm}^{-1}$ . A similar phenomenon has been reported in theoretical research on Sn isotopes [16],

wherein a linear correlation between the ratio of energy weighted sum rule exhausted by PDR over GDR and neutron skin thickness is found in  $^{106-120}\text{Sn}$ . In Ref. [20], the PDR fraction of photo-absorption cross section is linearly correlated to neutron skin thickness with a universal slope  $0.18-0.20 \text{ fm}^{-1}$  in ultra neutron-rich nuclei, which is smaller than our result. This discrepancy is mainly because they adopt the Skyrme functional SkM\* interaction [38] with incompressibility  $K_0 \approx 217 \text{ MeV}$  [39], which is softer than the relativistic non-linear meson-exchange model we used (NL3), with  $K_0 \approx 271 \text{ MeV}$  [40].

While in the second isotopic chain  $^{70-78}\text{Ni}$  the PDR peak is not well-defined, there is an overlap region between the PDR and GDR. Therefore, the value of integral cross section depends on the cutoff. In Fig. 4(c) the diamonds represent the result corresponding to cutoff 10 MeV, and squares for 11 MeV. The two sets of cross sections differ by about 1% of the total value. Nevertheless, they both break away from the linear correlation found in  $^{58-68}\text{Ni}$ , namely, although the neutron skin thickness increases with the number of valence neutrons monotonously, see Fig. 2(c), the growth of the PDR is stagnant.

The excess neutrons in nickel isotopes are filled in the major shell  $pf$  with the intruder  $1g_{9/2}$ . The E1 transitions have negative parity, which limits the final states of in-shell excitation to intruder orbits only, which have the desired opposite parity. That is the situation in  $^{58-68}\text{Ni}$ . Neutrons in  $2p_{3/2}, 2p_{1/2}, 1f_{5/2}$  orbits can be excited to  $1g_{9/2}$ . With the increasing number of valence nucleons, the gap between the outermost nucleons and the intruder orbit  $1g_{9/2}$  becomes smaller, and the transition gets easier. When the  $pf$  orbits are filled, i.e., nuclei  $^{66,68}\text{Ni}$ , the transition reaches a maximum. As a result, in the first group of Fig. 4, namely,  $^{58-68}\text{Ni}$ , the fraction of PDR integral cross section increases linearly with neutron skin thickness. As for nuclei  $^{70-78}\text{Ni}$ , the weakest bound nucleons lie in  $1g_{9/2}$ . For these neutrons, in-shell excitation is impossible, and the lowest available final state is the intruder orbit  $1h_{11/2}$  of the next major shell  $sdg$ , which often corresponds to large gaps and restrains the transition. In such a case, the pygmy dipole resonance consists of a competition between  $pf \rightarrow 1g_{9/2}$  and  $1g_{9/2} \rightarrow 1h_{11/2}$  excitations. The gap between  $1g_{9/2}$  and  $1h_{11/2}$  is larger than that between  $pf$  and  $1g_{9/2}$ ; the former is a  $1\hbar\omega$  excitation while the latter is  $0\hbar\omega$ . The neutrons in  $1g_{9/2}$  are not active when compared with lower levels; they play the role of PIEN. This is why neutron skin thickness increases but the growth of the pygmy resonance is stagnant.

Table 1.  $R_h^1$  of different nuclei. The second column is the outermost orbit  $l$  (in brackets is the number of neutrons in this orbit  $n_l$ ). The contributions of the neutrons in  $l$  are added up in the third column. The fourth and fifth columns contain the contribution of other valence neutrons and core neutrons, while the last column contains the contribution from proton excitation.

	$l$	$R_l(\%)$	$R_{V/l}(\%)$	$R_{\text{core}}(\%)$	$R_{\text{pro}}(\%)$
Ni58	$1f_{5/2}(2)$	68.64	0.00	12.50	18.86
Ni60	$1f_{5/2}(4)$	61.14	0.00	6.76	32.10
Ni62	$1f_{5/2}(6)$	71.62	0.00	13.00	15.38
Ni64	$2p_{3/2}(2)$	19.50	68.48	4.84	7.18
Ni66	$2p_{3/2}(4)$	50.79	43.50	3.19	2.53
Ni68	$2p_{1/2}(2)$	40.13	51.76	4.74	3.37
Ni70	$1g_{9/2}(2)$	2.56	92.10	2.65	2.69
Ni72	$1g_{9/2}(4)$	5.66	85.60	2.43	6.31
Ni74	$1g_{9/2}(6)$	4.89	91.25	0.91	2.95
Ni76	$1g_{9/2}(8)$	14.91	80.27	1.34	3.47
Ni78	$1g_{9/2}(10)$	13.01	82.41	0.00	4.58

The contribution of a hole state  $h$  to the PDR can be measured using Eq. (16) by restricting the sum in the PDR energy region. In nickel isotopes with mass 70-78, the outermost neutrons occupy orbit  $1g_{9/2}$  sequentially. From Table 1, in these nuclei the contribution of neutrons in core  $^{56}\text{Ni}$  to the PDR are quite small, in general less than 3%, while the protons contribute no

more than 6.5%, so the PDR is mainly aroused by excitation of excess valence neutrons. What is important to the stagnancy is the sudden drop in the  $1g_{9/2}$  orbit's contribution. When the number of excess neutrons increases, the resonance becomes more and more collective. The transition strength is distributed over each excess neutron, but neutrons in  $1g_{9/2}$  are exceptional. The averaged contribution of each neutron in  $1g_{9/2}(R_l/n_l)$  is about 0.81%–1.86%, far less than that of other lower orbit valence neutrons, which have average values about 6.69%–7.67% ( $n_{V/l} = 12$ ). The transition contributions relating to  $1g_{9/2}$  participating p-h pairs are relatively small. In other words, they form an inertial skin covering the outside of the nucleus that cannot be excited easily.

Similarly, the contribution of a hole state  $h$  to the whole dipole excitation can be measured by counting all the excited states in Eq. (16), i.e., letting  $\nu \in [0, \infty]$ . The corresponding results are listed in Table 2. The nucleons in the  $^{56}\text{Ni}$  core are still suppressed, mainly because of the large gaps, and the protons have a larger contribution. The averaged transition contribution of  $1g_{9/2}$  neutrons is 1.95%–4.34%, while that for other valence neutrons is 2.84%–4.02%, namely, there's no significant preference between these two groups. From Fig. 3(c) we can also learn that the collectivities of the GDR increase continuously in  $^{70-78}\text{Ni}$ , and the suppression effect of  $1g_{9/2}$  does not show up. Therefore, we can conclude that the inertial skin only matters in the PDR. The neutrons in the  $1g_{9/2}$  orbital are PIEN, but are not inertial in the whole dipole excitation.

Table 2. The same as Table 1, except the excitation levels are summed up over the whole spectrum.

	$l$	$R_l(\%)$	$R_{V/l}(\%)$	$R_{\text{core}}(\%)$	$R_{\text{pro}}(\%)$
Ni70	$1g_{9/2}(2)$	8.67	39.28	15.17	36.89
Ni72	$1g_{9/2}(4)$	12.14	48.26	15.76	23.84
Ni74	$1g_{9/2}(6)$	17.93	35.61	16.05	30.41
Ni76	$1g_{9/2}(8)$	18.64	36.19	12.53	32.64
Ni78	$1g_{9/2}(10)$	19.52	34.11	9.77	36.60

## 5 Conclusion

The RPA method is an important tool in the study of nuclear low-lying excitation properties. In this work, we have finished a new numerical implementation of an axial-deformed random phase approximation method based on the relativistic meson-exchange model. Under such a formalism, we studied the pygmy dipole excitation of even-even neutron-rich nickel isotopes. The PDR is of isoscalar nature and can be explained as the excitations of excess neutrons against the isospin saturated core. In this mode, neutrons and protons are oscillating in-phase in the inner region, while in the surface area,

only neutrons oscillate. The collectivity of the PDR is much weaker than that of the GDR. With our introduced indicator, we also found when the number of excess neutrons increases, the PDR becomes more collective, but in  $^{70-78}\text{Ni}$  the degree of collectivity does not increase further, which implies there is an inactive part in those valence neutrons (PIEN). The magnitude of the PDR is related to neutron skin thickness. In our study, a linear correlation between neutron skin thickness and PDR integral photo-absorption cross section has been found when the excess neutrons lie in  $pf$  orbits. However, when the nucleus become more neutron-rich, e.g.,  $^{70-78}\text{Ni}$ , despite the neutron skin increasing monotonically,

the PDR growth is stagnant. This is because for these nuclei, neutrons in orbit  $1g_{9/2}$  are less active and form an inertial skin, preventing in-phase excitations of neutrons and protons. This can be understood by noticing the sudden drop of the transition contributions belonging to  $1g_{9/2}$  valence neutrons.

*Our RPA program requires the single particle wave-functions of the RMF code RMFAXIAL developed by P. Ring et al. [32] as inputs. We accessed the RMF code from the Computer Physics Communications Program Library under the non-profit use licence agreement, and really appreciate their work.*

## References

- 1 T. Hartmann, J. Enders, P. Mohr et al, Phys. Rev. Lett., **85**: 274 (2000)
- 2 P. Adrich, A. Klimkiewicz, M. Fallot et al, Phys. Rev. Lett., **95**: 132501 (2005)
- 3 O. Wieland, A. Bracco, F. Camera et al, Phys. Rev. Lett., **102**: 092502 (2009)
- 4 D. Vretenar, N. Paar, P. Ring et al, Nuclear Physics A, **692**(3): 496 (2001)
- 5 N. Paar, D. Vretenar, E. Khan et al, Reports on Progress in Physics, **70**(5): 691 (2007)
- 6 H. Sagawa, N. Van Giai, N. Takigawa et al, Zeitschrift für Physik A Hadrons and Nuclei, **351**(4): 385 (1995)
- 7 J. Endres, E. Litvinova, D. Savran et al, Phys. Rev. Lett., **105**: 212503 (2010)
- 8 J. Endres, D. Savran, A. M. v. d. Berg et al, Phys. Rev. C, **80**: 034302 (2009)
- 9 E. G. Lanza, A. Vitturi, E. Litvinova et al, Phys. Rev. C, **89**: 041601 (2014)
- 10 G. Rusev, R. Schwengner, F. Dönau et al, Phys. Rev. C, **77**: 064321 (2008)
- 11 J. Gibelin, D. Beaumel, T. Motobayashi et al, Phys. Rev. Lett., **101**: 212503 (2008)
- 12 B. Lauther, D. Savran, T. Aumann et al, Physics Letters B, **756**: 72 (2016)
- 13 M. Scheck, V. Y. Ponomarev, T. Aumann et al, Phys. Rev. C, **87**: 051304 (2013)
- 14 S. Goriely, Physics Letters B, **436**(1): 10 (1998)
- 15 A. Carbone, G. Colò, A. Bracco et al, Phys. Rev. C, **81**: 041301 (2010)
- 16 J. Piekarewicz, Phys. Rev. C, **73**: 044325 (2006)
- 17 C. Xu, Z. Ren, and J. Liu, Phys. Rev. C, **90**: 064310 (2014)
- 18 V. Baran, M. Colonna, M. Di Toro et al, Phys. Rev. C, **88**: 044610 (2013)
- 19 T. Shizuma, T. Hayakawa, H. Ohgaki et al, Phys. Rev. C, **87**: 024301 (2013)
- 20 T. Inakura, T. Nakatsukasa, and K. Yabana, Phys. Rev. C, **84**: 021302 (2011)
- 21 J. Boguta and A. Bodmer, Nuclear Physics A, **292**(3): 413 (1977)
- 22 D. Vretenar, A. Afanasjev, G. Lalazissis et al, Physics Reports, **409**(34): 101 (2005)
- 23 P. Ring and P. Schuck, *The Nuclear Many-Body Problem*. Springer (2004)
- 24 N. Paar, P. Ring, T. Nikšić et al, Phys. Rev. C, **67**: 034312 (2003)
- 25 S. Ebata, T. Nakatsukasa, T. Inakura et al, Phys. Rev. C, **82**: 034306 (2010)
- 26 D. P. n. Arteaga, E. Khan, and P. Ring, Phys. Rev. C, **79**: 034311 (2009)
- 27 J. Piekarewicz, Phys. Rev. C, **83**: 034319 (2011)
- 28 P. Ring, Z. Y. Ma, N. V. Giai et al, Nuclear Physics A, **694**(1): 249 (2001)
- 29 D. Yang, L.-G. Cao, Y. Tian et al, Phys. Rev. C, **82**: 054305 (2010)
- 30 Ding Yang, Li-Gang Cao, and Zhong-Yu Ma, Chinese Physics C, **37**(12): 124102 (2013)
- 31 D. P. Arteaga and P. Ring, Phys. Rev. C, **77**: 034317 (2008)
- 32 P. Ring, Y. Gambhir, and G. Lalazissis, Computer Physics Communications, **105**(1): 77 (1997)
- 33 T. Niki, N. Paar, D. Vretenar et al, Computer Physics Communications, **185**(6): 1808 (2014)
- 34 N. Paar, Y. F. Niu, D. Vretenar et al, Phys. Rev. Lett., **103**: 032502 (2009)
- 35 H. Nakada, T. Inakura, and H. Sawai, Phys. Rev. C, **87**: 034302 (2013)
- 36 N. Tsoneva and H. Lenske, Phys. Rev. C, **77**: 024321 (2008)
- 37 G. Co', V. De Donno, M. Anguiano et al, Phys. Rev. C, **87**: 034305 (2013)
- 38 J. Bartel, P. Quentin, M. Brack et al, Nuclear Physics A, **386**(1): 79 (1982)
- 39 L.-G. Cao, H. Sagawa, and G. Colò, Phys. Rev. C, **86**: 054313 (2012)
- 40 B.-A. Li, L.-W. Chen, and C. M. Ko, Physics Reports, **464**(46): 113 (2008)